

## Muon spin relaxation study of the layered kagome superconductor $\text{CsV}_3\text{Sb}_5$

Zhaoyang Shan,<sup>1,2</sup> Pabitra K. Biswas,<sup>3,\*</sup> Sudeep K. Ghosh<sup>4,5,†</sup>, T. Tula<sup>6,5</sup>, Adrian D. Hillier<sup>6,3</sup>, Devashibhai Adroja<sup>6,3,6</sup>, Stephen Cottrell,<sup>3</sup> Guang-Han Cao,<sup>1,2,7</sup> Yi Liu,<sup>8</sup> Xiaofeng Xu<sup>8</sup>, Yu Song,<sup>1,2</sup> Huiqiu Yuan,<sup>1,2,7,9</sup> and Michael Smidman<sup>1,2,‡</sup>

<sup>1</sup>Center for Correlated Matter and Department of Physics, Zhejiang University, Hangzhou 310058, China

<sup>2</sup>Zhejiang Province Key Laboratory of Quantum Technology and Device, Department of Physics, Zhejiang University, Hangzhou 310058, China

<sup>3</sup>ISIS Facility, STFC Rutherford Appleton Laboratory, Harwell Science and Innovation Campus, Didcot OX11 0QX, United Kingdom

<sup>4</sup>Department of Physics, Indian Institute of Technology, Kanpur 208016, India

<sup>5</sup>School of Physical Sciences, University of Kent, Canterbury CT2 7NH, United Kingdom

<sup>6</sup>Highly Correlated Matter Research Group, Physics Department, University of Johannesburg, P.O. Box 524, Auckland Park 2006, South Africa

<sup>7</sup>State Key Laboratory of Silicon Materials, Zhejiang University, Hangzhou 310058, China

<sup>8</sup>Key Laboratory of Quantum Precision Measurement of Zhejiang Province, Department of Applied Physics, Zhejiang University of Technology, Hangzhou 310023, China

<sup>9</sup>Collaborative Innovation Center of Advanced Microstructures, Nanjing University, Nanjing 210093, China



(Received 11 March 2022; revised 30 May 2022; accepted 1 August 2022; published 23 August 2022)

The  $\mathbb{Z}_2$  topological metals  $RV_3\text{Sb}_5$  ( $R = \text{K}, \text{Rb}, \text{Cs}$ ) with a layered kagome structure provide a unique opportunity to investigate the interplay between charge order, superconductivity, and topology. Here, we report muon-spin relaxation/rotation ( $\mu\text{SR}$ ) measurements performed on  $\text{CsV}_3\text{Sb}_5$  across a broad temperature range, in order to uncover the nature of the charge density wave order and superconductivity in this material. From zero-field  $\mu\text{SR}$ , we find that spontaneous magnetic fields appear below 50 K, which is well below the charge density wave transition ( $T^* \sim 93$  K). We show that these spontaneous fields are dynamic in nature making it difficult to associate them with a hidden static order. The superconducting state of  $\text{CsV}_3\text{Sb}_5$  is found to preserve time-reversal symmetry, and the transverse-field  $\mu\text{SR}$  results are consistent with a superconducting state that has two fully open gaps.

DOI: [10.1103/PhysRevResearch.4.033145](https://doi.org/10.1103/PhysRevResearch.4.033145)

### I. INTRODUCTION

Kagome lattice compounds have served as ideal platforms for exploring both unusual magnetic phenomena, such as geometric frustration and quantum spin liquids [1–3], and electronic behaviors due to the presence of flat bands, Dirac cones, and nontrivial band topologies [4–7]. The recently discovered superconductors  $RV_3\text{Sb}_5$  ( $R = \text{K}, \text{Rb}, \text{Cs}$ ) have therefore attracted much attention for the study of superconductivity in kagome lattice systems [8–11], which have topological band structures with multiple Dirac cones. These materials also exhibit unusual charge density wave (CDW) ordering, which is accompanied by a giant anomalous Hall effect [12,13], and in  $\text{KV}_3\text{Sb}_5$  was reported to correspond

to a chiral charge ordering [14]. Moreover, this CDW order exhibits clear competition with the superconductivity in these compounds, where there is an enhancement of  $T_c$  upon the suppression of the CDW state by pressure [15–22]. Although low-temperature thermal conductivity measurements suggested a nodal superconducting gap in  $\text{CsV}_3\text{Sb}_5$  [23], penetration depth measurements using the tunnel-diode oscillator (TDO) and muon-spin rotation methods [24,25] as well as scanning tunneling microscopy, point contact spectroscopy, and nuclear magnetic/quadrupole resonance [26–30] point to fully gapped multiband superconductivity with a sign-preserving order parameter.

Given the unconventional properties of the CDW state, together with various theoretical proposals including chiral flux phases and star of David and inverse star of David configurations [31–34], it is important to probe whether time-reversal symmetry (TRS) is broken in the CDW state. In the case of  $\text{KV}_3\text{Sb}_5$ , an enhanced relaxation rate of the asymmetry from muon-spin relaxation ( $\mu\text{SR}$ ) is detected below the CDW transition  $T^* = 80$  K [35], corresponding to the spontaneous appearance of static magnetic fields. On the other hand, in  $\text{CsV}_3\text{Sb}_5$  the enhanced relaxation rate was found to have its onset well below the CDW transition  $T^* = 93$  K [36], while no evidence for TRS breaking along the  $c$  axis could be

\*pabitra.biswas@stfc.ac.uk

†S.Ghosh@kent.ac.uk

‡msmidman@zju.edu.cn

Published by the American Physical Society under the terms of the [Creative Commons Attribution 4.0 International](https://creativecommons.org/licenses/by/4.0/) license. Further distribution of this work must maintain attribution to the author(s) and the published article's title, journal citation, and DOI.

detected with spin-polarized tunneling spectroscopy [37]. As such, it is of particular interest to further examine the nature of the spontaneous fields emerging within the charge ordered state.

Here, we report muon-spin relaxation/rotation measurements of  $\text{CsV}_3\text{Sb}_5$  in zero, longitudinal, and transverse magnetic fields. We observe an increase in the  $\mu\text{SR}$  relaxation rate upon cooling in zero field, which is significantly enhanced below around 50 K, well below  $T^* \sim 93$  K. This enhancement persists in a 50 G longitudinal field, pointing to the dynamic nature of these fields. Measurements in the superconducting state indicate the lack of additional spontaneous fields appearing below the superconducting transition, and the superfluid density derived from transverse-field results is consistent with the previously observed multiband superconductivity.

## II. EXPERIMENTAL DETAILS

Polycrystalline samples of  $\text{CsV}_3\text{Sb}_5$  were prepared by a solid-state reaction method. Stoichiometric amounts of Cs (liquid, Alfa 99.98%), V (powder, Sigma 99.9%), and Sb (shot, Alfa 99.999%) were mixed thoroughly in a glovebox filled with Ar gas. The mixture was subsequently loaded in an alumina crucible that was then jacketed in a tantalum tube. The tantalum tube was thereafter sealed in an evacuated quartz ampoule, heated up to 600 °C, and held at this temperature for 3 days, before being furnace cooled to room temperature. The single phase of the as-grown samples was checked by powder x-ray diffraction on a PANalytical x-ray diffractometer with monochromatic  $\text{Cu-K}\alpha_1$  radiation.  $\mu\text{SR}$  measurements were performed on powdered  $\text{CsV}_3\text{Sb}_5$  samples at the ISIS facility at elevated temperatures between 5 and 180 K using the EMU spectrometer in a  $^4\text{He}$  cryostat, and at low temperatures down to 0.1 K in a dilution refrigerator using the MuSR spectrometer. For zero-field (ZF) and longitudinal-field (LF) measurements, the asymmetry  $A(t)$  between the number of positrons detected at the forward ( $N_F$ ) and backward ( $N_B$ ) positions was analyzed via

$$A(t) = \frac{N_F - \alpha N_B}{N_F + \alpha N_B}, \quad (1)$$

where  $\alpha$  is a calibration constant. For transverse-field (TF) measurements, the time-dependent histograms corresponding to 16 groups of detectors were simultaneously analyzed using the MUSRFIT software package [38].

## III. RESULTS AND DISCUSSION

### A. Zero- and longitudinal-field $\mu\text{SR}$ at elevated temperatures

Figure 1(a) displays the  $\mu\text{SR}$  spectra at several selected temperatures, measured in zero applied field on the EMU spectrometer. It can be seen that upon reducing the temperature, there is an increase in the relaxation rate of the asymmetry, indicating a broadening of the internal field distribution at the muon-stopping site. The shape of the muon spectra is indicative of a Kubo-Toyabe relaxation function, arising from a Gaussian distribution of magnetic fields static on the timescale of the muon lifetime ( $2.2 \mu\text{s}$ ). The data were analyzed taking into account both Gaussian Kubo-Toyabe (GKT)

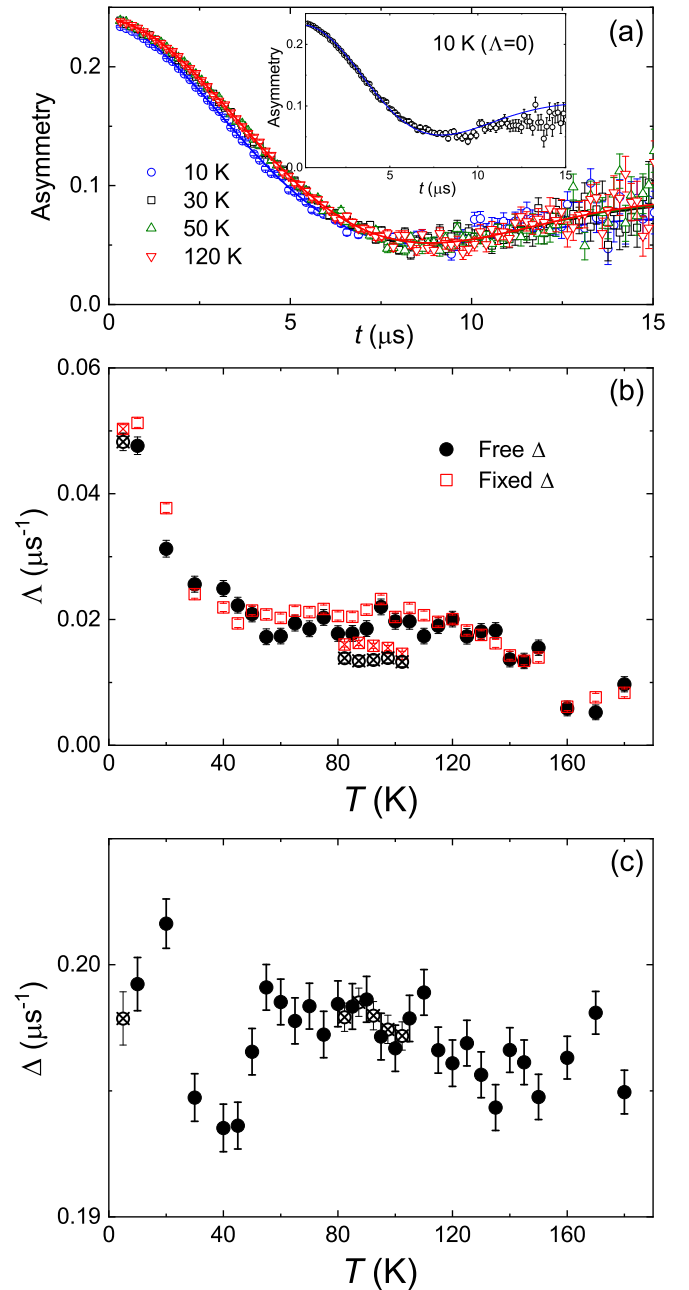


FIG. 1. (a) Zero-field  $\mu\text{SR}$  measurements of  $\text{CsV}_3\text{Sb}_5$  measured at four temperatures, where the solid curves show the results from fitting using Eq. (2). The inset shows the data at 10 K, where the blue solid curve shows the results of fitting using Eq. (2) with  $\Lambda = 0$ . It can be seen that in the inset there is considerable deviation of the fitting from the data, showing the necessity of considering an exponential relaxation channel [39]. (b) and (c) The temperature dependence of the fitted values of the exponential relaxation rate  $\Lambda$  (b) and the Kubo-Toyabe relaxation rate  $\Delta$  (c). The values of  $\Lambda$  are shown for both the case where  $\Delta$  is fitted as a free parameter and the case where  $\Delta$  is fixed to the value obtained at 120 K. The symbols filled with a cross correspond to points which were measured in ZF after a LF had been applied, as described in the text.

and exponential relaxation channels ( $e^{-\Lambda t}$ ) via

$$A(t) = A\left[\frac{1}{3} + \frac{2}{3}(1 - \Delta^2 t^2)e^{-\Delta^2 t^2/2}\right]e^{-\Lambda t} + A_{\text{BG}}, \quad (2)$$

where  $A$  and  $A_{BG}$  correspond to the initial asymmetries for muons stopping in the sample and silver sample holder, respectively, which were fixed to the fitted values at 120 K, while  $\Delta$  and  $\Lambda$  are the Gaussian Kubo-Toyabe and exponential relaxation rates. Note that if a purely Gaussian relaxation is considered ( $\Lambda = 0$ ), the low-temperature spectra cannot be well fitted, as can be seen in the inset of Fig. 1(a), where there is a systematic deviation of the fit from the data at 10 K [39]. In addition to the deviation at low times below  $0.6 \mu\text{s}$ , it can also be seen that the fitted curve undershoots the data between 4.5 and  $8 \mu\text{s}$ , while it overshoots at longer times. This suggests that an exponential relaxation channel is also essential to fully describe the low-temperature relaxation of  $\text{CsV}_3\text{Sb}_5$ , as was also found for  $\text{KV}_3\text{Sb}_5$  [35] and  $\text{RbV}_3\text{Sb}_5$  [40].

The temperature dependence of the fitted values of  $\Lambda$  and  $\Delta$  between 5 and 180 K are displayed in Figs. 1(b) and 1(c), respectively. It can be seen that there is little change in  $\Delta$  with temperature. On the other hand, at the highest temperatures,  $\Lambda$  is small, indicating that the relaxation is nearly entirely from the nuclear moments which are static on the timescale of the muon lifetime. Upon lowering the temperature, there is an onset of the exponential component below around 160 K, with little change across the intermediate temperature range. Below around 50 K, there is a significant increase in  $\Lambda$ , which continues to increase with decreasing temperature down to the lowest measured temperature (5 K). To check that this low-temperature increase in  $\Lambda$  is not an artifact of correlations between the  $\Lambda$  and  $\Delta$  parameters, the data were fitted with  $\Delta$  fixed to the value at 120 K ( $\Delta = 0.1961 \mu\text{s}^{-1}$ ). As shown in Fig. 1(b), a very similar trend is still observed in  $\Lambda$ , showing the intrinsic nature of this low-temperature enhancement of the relaxation. We note that  $\Lambda$  is very small above around 150 K, and the data here are well accounted for by only a static relaxation function. This suggests that the low-temperature increase in  $\Lambda$  is not due to the slowing down of thermal muon diffusion processes, since such thermally activated hopping of the muons would also be expected to lead to dynamic behavior at higher temperatures, as well as a significant temperature dependence, which is not observed in the intermediate temperature range (60–140 K).

Note that in Fig. 1(b) a few points (filled with a cross) are systematically lower than the adjacent values. These were measured after a longitudinal field had been applied and then removed at low temperatures, pointing to a weak dependence of this component on the field history. These results therefore show that there is a significant increase in the low-temperature relaxation, which occurs well below the charge ordering transition at  $T^* = 93$  K. This is different from that observed in  $\mu\text{SR}$  measurements of isostructural  $\text{KV}_3\text{Sb}_5$  [35], where an enhanced relaxation in the exponential channel had its onset at  $T^* = 80$  K, but is similar to another study of  $\text{CsV}_3\text{Sb}_5$  where the increase had its onset at around 70 K, also below the charge ordering temperature, which is reported as evidence for a hidden flux phase [36]. However, in Ref. [36] the relaxation corresponding to muons stopping in  $\text{CsV}_3\text{Sb}_5$  is ascribed to purely Gaussian relaxation, whereas here we find that both exponential and Gaussian components are required to account for our data, and the low-temperature increase is predominantly in the exponential relaxation rate.

Since the analysis of the ZF- $\mu\text{SR}$  data in the normal state of  $\text{CsV}_3\text{Sb}_5$  using Eq. (2) implies that both the Gaussian and Lorentzian relaxation channels are present, we complement this analysis by a recently introduced unbiased principal component analysis (PCA) technique [41]. PCA is a simple unsupervised machine learning (model independent) technique used for reducing dimensionality of the data. In the PCA technique, a linear transformation in the data space is used to find only a few orthonormal basis vectors called principal components (PCs) such that they can well capture the covariance of the data with respect to the average. The projections of the original data on the PCs are called the PC scores. Changes in values of the most important PC scores, which capture most covariance in the data, reflect crucial changes between asymmetry functions at different temperatures. This technique has recently been successfully used to identify transitions that are associated with TRS breaking in superconductors from ZF- $\mu\text{SR}$  data of  $\text{LaNiGa}_2$ , and  $\text{LaNi}_{1-x}\text{Cu}_x\text{C}_2$  [42], although the changes in these cases can be subtle, and magnetic transitions in antiferromagnetic  $\text{BaFe}_2\text{Se}_2\text{O}$ . We note that although this method can successfully determine changes in the asymmetry function by corresponding changes in the principal component scores and hence can complement the standard regression analysis, it is difficult to associate those changes with any particular type of relaxation channel.

We show the results of PCA in Fig. 2 for  $\text{CsV}_3\text{Sb}_5$  performed jointly on ZF- $\mu\text{SR}$  data from several materials showing TRS breaking [42]. We first identify the PCs that have the largest contributions to the covariance of the  $\text{CsV}_3\text{Sb}_5$  data by computing the cumulative principal component score (cPCS) metric [43]. The cumulative PC scores for  $\text{CsV}_3\text{Sb}_5$  are shown in Fig. 2(a). We note that only the first three PCs are important and the first PC captures the most covariance of the data. We have computed the error bars in the PC scores by assuming that the errors come solely from the experimental errors of the asymmetry functions. The PC scores at a given temperature are defined as

$$\text{PC}_{\text{score}}^{[n]}(T_i) = \sum_j^M \text{PC}^{[n]}(t_j) \times A(T_i, t_j), \quad (3)$$

where  $\text{PC}^{[n]}(t_j)$  is a value of the  $n$ th PC at time  $t_j$ . Assuming that errors coming from different time windows are not correlated, we obtain the PC score standard deviation as

$$\text{SD}[\text{PC}_{\text{score}}^{[n]}(T_i)] = \sqrt{\sum_j^M (\text{PC}^{[n]}(t_j) \times E(T_i, t_j))^2}, \quad (4)$$

where  $E(T_i, t_j)$  indicates the experimental error of the asymmetry function  $A(T_i, t_j)$  and we also assume that the error coming from the variation of  $\text{PC}^{[n]}(t_j)$  is negligible.

We note from the variations of the PC scores as a function of temperature shown in Figs. 2(b)–2(d) that all of the three PCs show a clear and significant change below  $T \approx 50$  K. The changes in the PC scores set in below  $T \approx 160$  K, where in the intermediate temperature range there is little variation in the second and third PCs, while the first PC has a clear shoulder at around 100 K close to  $T^*$ , suggesting a relationship between the additional fields and the charge ordering. Thus the PCA corroborates the results of the previous analysis of

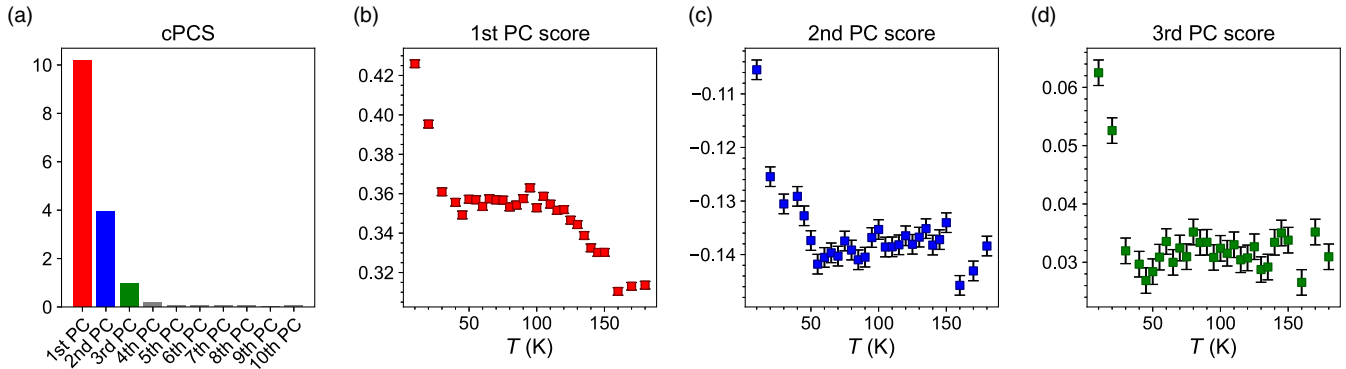


FIG. 2. Principal component analysis (PCA) of the ZF- $\mu$ SR spectra of CsV<sub>3</sub>Sb<sub>5</sub> in the normal state. (a) Cumulative principal component score for each PC. The first three PCs have the largest contribution to the data reconstruction. (b)–(d) Principal component scores for the first, second, and third most important PCs as functions of temperature.

ZF- $\mu$ SR data using Eq. (2) showing the onset of additional fields below  $T \approx 50$  K, which may be associated with spontaneous fields in the charge ordered state.

While an exponential relaxation is often interpreted as arising from fluctuating internal fields, it can also correspond to a Lorentzian distribution of static fields, as reported for KV<sub>3</sub>Sb<sub>5</sub> [35], as well as several time-reversal symmetry breaking superconductors [44–48]. To distinguish between these two scenarios, we performed measurements in a LF of 50 G, which are displayed for three temperatures in Fig. 3(a). It can be seen that a significant relaxing component is still observed in this LF, and the relaxation rate increases with decreasing temperature, while the Kubo-Toyabe component observed in ZF is absent, as expected when the muons are decoupled from this relaxation channel. When a larger LF of 500 G is applied, the muons are nearly entirely decoupled from the local fields even at 5 K, with only a very small drop in the asymmetry.

The 50 G data were analyzed using

$$A(t) = Ae^{-\Lambda_L t} + A_{BG}, \quad (5)$$

where  $A_{BG}$  was fixed to the same value as the ZF analysis. The temperature dependence of  $\Lambda_L$  in the 50 G LF is displayed in Fig. 3(b), where a sizable value is still observed at low and intermediate temperatures. Furthermore, the significant low-temperature enhancement observed below 50 K in the ZF data is still present in a LF of 50 G. If the relatively small internal fields detected in the ZF measurements were purely static, they would be expected to be entirely decoupled by the LF, as was observed for KV<sub>3</sub>Sb<sub>5</sub> in a 25 G LF [49], and this therefore suggests that the exponential component for CsV<sub>3</sub>Sb<sub>5</sub> corresponds to fluctuating magnetic fields and, as such, the low-temperature enhancement also has a dynamic nature. The dependence of  $\Lambda_L$  on the applied LF ( $B_L$ ) in the fast-fluctuation limit can be estimated using the Redfield formula

$$\Lambda_L = \frac{\Lambda v^2}{\gamma_\mu^2 B_L^2 + v^2}, \quad (6)$$

where  $\Lambda$  is the value in ZF. Using the 5 K values of  $\Lambda = 0.04825 \mu\text{s}^{-1}$  and  $\Lambda_L = 0.01875 \mu\text{s}^{-1}$  for the 50 G LF, we estimate  $v = 3.39 \mu\text{s}^{-1}$ , corresponding to a correlation time  $\tau_c = 0.29 \mu\text{s}$ . The magnitude of the local fields  $B_{\text{loc}}$  can be related to  $\Lambda$  via  $\Lambda = 2(\gamma_\mu B_{\text{loc}})^2/v$ , yielding  $B_{\text{loc}} \approx 3$  G. These are similar local fields and correlation times inferred for the dynamic part of the  $\mu$ SR spectra of PrOs<sub>4</sub>Sb<sub>12</sub> [50], which were suggested to reflect the  $4f$ -electron dynamics of the system.

Due to the intriguing dynamic nature of the spontaneous fields below 50 K inside the CDW phase, it is difficult to associate them with a hidden static order, such as the one proposed in Ref. [36]. This further validates the unconventional nature of the CDW phase in CsV<sub>3</sub>Sb<sub>5</sub> reported by other measurements such as pump-probe spectroscopy [51,52]. It was found that there is a change in rotational symmetry below 50 K from  $C_6$  to  $C_2$  which is more like a crossover and the electronic and orbital degrees of freedom curiously behave differently in this regime [52]. In addition, our measurements do not show the second transition below 30 K reported in Ref. [36]. Further experimental and theoretical studies are therefore necessary to uncover the true nature of the

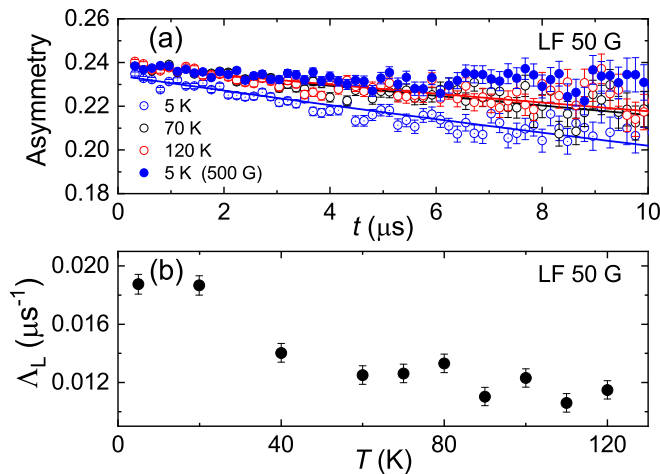


FIG. 3. (a)  $\mu$ SR measurements of CsV<sub>3</sub>Sb<sub>5</sub> performed in longitudinal applied fields, where the open symbols correspond to data at three temperatures in a longitudinal field of 50 G, while the solid symbols correspond to measurements in a 500 G field, where the muons are decoupled from the local fields. The solid lines show the results from fitting the 50 G data using Eq. (5). (b) Temperature dependence of the exponential relaxation rate  $\Lambda_L$  obtained from analyzing the data in the 50 G LF.



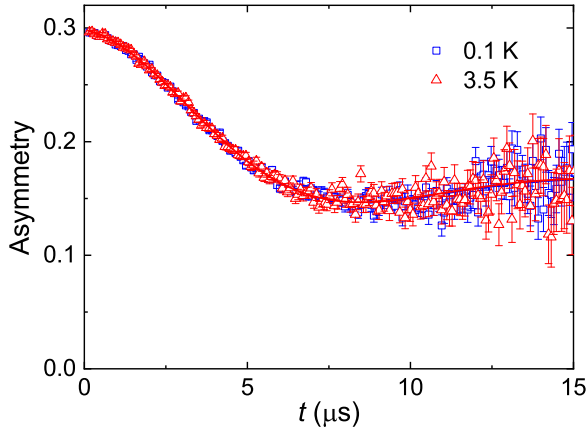


FIG. 4. Zero-field  $\mu$ SR measurements performed on the MuSR spectrometer both in the normal state at 3.5 K and far below the superconducting transition at 0.1 K. The solid curves show the results from fitting using Eq. (2).

spontaneous fields associated with the CDW phase in  $\text{CsV}_3\text{Sb}_5$ . We note that in 1T-TaS<sub>2</sub>, changes in the LF- $\mu$ SR spectra at different temperatures within the CDW phase were associated with the diffusion of spinons in distinct quantum spin liquid states [53]. In addition, the dynamic fields observed in  $\text{CsV}_3\text{Sb}_5$  are distinct from the static spontaneous fields inferred to appear at the charge order transition of isostructural  $\text{KV}_3\text{Sb}_5$  [35,49]. This points to fundamental differences in the charge ordered states of the two compounds, which could potentially arise from the presence of different types of Van Hove singularity [54].

### B. $\mu$ SR measurements in the superconducting state

In order to search for the appearance of spontaneous magnetic fields in the superconducting state, indicative of a TRS breaking pairing state [55], ZF- $\mu$ SR was measured using the MuSR spectrometer with the sample cooled in a dilution refrigerator. Figure 4 displays spectra measured in ZF at two temperatures, at 3.5 K in the normal state and at 0.1 K well below  $T_c$ , where there is little difference between the measurements at the two temperatures. The data were fitted using Eq. (2), yielding  $\Delta = 0.205(2) \mu\text{s}^{-1}$  and  $\Lambda = 0.039(3) \mu\text{s}^{-1}$  for both temperatures. These fitting results suggest a lack of additional magnetic fields in the superconducting state, indicating that the pairing state does not break TRS, consistent with previous results for both  $\text{CsV}_3\text{Sb}_5$  and  $\text{KV}_3\text{Sb}_5$  [25,35].

To determine the temperature dependence of the superfluid density, muon-spin rotation measurements were performed in a TF of 300 G, as shown for two temperatures in Fig. 5. An increased relaxation in the superconducting state corresponds to the formation of a flux-line lattice, which is sensitive to the magnitude of the penetration depth, and hence the superfluid density. The data were analyzed using

$$A_{\text{TF}}(t) = A_s e^{-\sigma^2 t^2 / 2} \cos(\gamma_\mu B_s t + \phi) + A_{bg} \cos(\gamma_\mu B_{bg} t + \phi), \quad (7)$$

where the first and second terms correspond to muons stopping in the sample and sample holder, respectively, and  $\phi$  is a common phase. Here, the ratio  $A_s/A_{bg}$  was fixed to the fitted

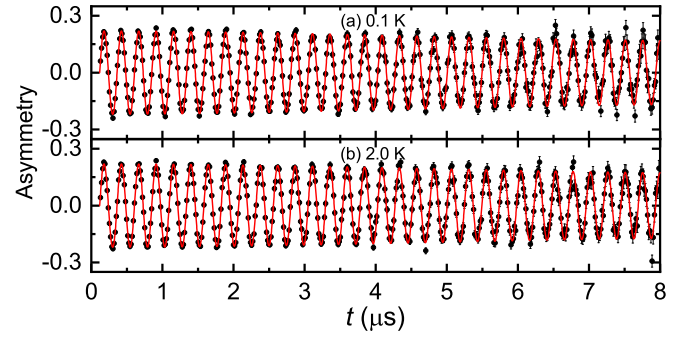


FIG. 5. Muon-spin rotation measurements of  $\text{CsV}_3\text{Sb}_5$  measured in a 300 G transverse field at (a) 0.1 K and (b) 2 K. The solid curves show the results from fitting using Eq. (7).

value obtained from fitting at the lowest measured temperature. The superconducting contribution to the relaxation  $\sigma_{sc}$  was calculated using  $\sigma_{sc} = \sqrt{\sigma^2 - \sigma_n^2}$ , using a normal state contribution  $\sigma_n = 0.209 \mu\text{s}^{-1}$  estimated from the normal state data. The temperature dependence of  $\sigma_{sc}$ , which is proportional to the superfluid density, is displayed in Fig. 6. A clear low-temperature saturation of  $\sigma_{sc}$  cannot be resolved, and the data cannot be accounted for using a single-gap  $s$ -wave model. On the other hand, there are not sufficient low-temperature data points to resolve whether at low temperatures the data do approach a constant value, as expected for a fully open superconducting gap, or whether they exhibit power-law behavior characteristic of nodal superconductivity. In a previous penetration depth study using the tunnel-diode oscillator based method [24], fully gapped behavior is revealed by  $\lambda(T)$  becoming flat only at very low temperatures, below around 0.2 K, and the data are analyzed using an isotropic two-gap  $s$ -wave model. Similarly, we fitted  $\sigma_{sc}$  with the same two-gap  $s + s$  model, which as shown by the red curve in Fig. 6 can well describe the data, with zero-temperature gap magnitudes of  $\Delta_1 = 0.55k_B T_c$  and  $\Delta_2 = 2.72k_B T_c$ , with a fraction corresponding to the smaller gap of 22%. Here, the value of the small gap is very close to that from the analysis of the TDO

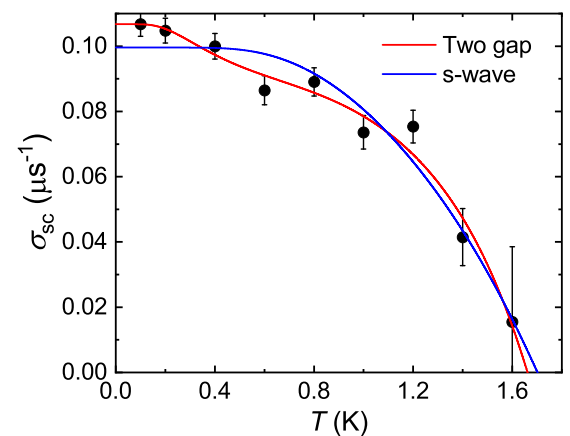


FIG. 6. Temperature dependence of  $\sigma_{sc}$  of  $\text{CsV}_3\text{Sb}_5$  determined from TF- $\mu$ SR results, which is proportional to the superfluid density. The solid curves show the results from fitting with a two-gap  $s$ -wave model and an isotropic  $s$ -wave model as described in the text.

data [24], while  $\Delta_2$  is larger, being closer to that deduced previously from  $\mu$ SR [25]. Therefore these results are consistent with the previous findings of two-gap superconductivity in  $\text{CsV}_3\text{Sb}_5$  [24,25].

The multigap superconductivity with preserved TRS found in  $\text{CsV}_3\text{Sb}_5$  constrains the forms of possible superconducting instabilities in conjunction with other measurements which indicate isotropic full gap behavior [24–30]. In particular, the proposed nodal  $f$ -wave-type [56] superconducting order parameter seems to be incompatible with the experimental observations in  $\text{CsV}_3\text{Sb}_5$ . Rather, a fully gapped superconducting state resulting from the multiband nature and an intricate interplay [54] between the CDW phase, superconductivity, and topological order is expected to be realized in  $\text{CsV}_3\text{Sb}_5$ , and further studies are necessary to uncover its true nature and pairing mechanism.

#### IV. CONCLUSION

In summary, we performed ZF-, LF-, and TF- $\mu$ SR measurements on the kagome lattice superconductor  $\text{CsV}_3\text{Sb}_5$ . Upon lowering the temperature, a significant increase in the relaxation rate corresponding to the exponential relaxation channel of the ZF asymmetry is observed, which has its onset below around 50 K, well below the charge ordering temperature  $T^* = 93$  K. Upon measuring in a LF of 50 G, a sizable relaxation is still observed, which also shows a sim-

ilar low-temperature increase, indicating the dynamic nature of these small fields. Meanwhile ZF measurements at lower temperatures show no detectable change upon entering the superconducting state, indicating that the superconducting order parameter does not break TRS, while the TF- $\mu$ SR analysis is consistent with the previous findings of two-gap  $s$ -wave superconductivity. While it is still an open question as to whether the additional internal fields that have their onset well below  $T^*$  are related to changes in the charge ordered state, the dynamic nature of these fields inferred from our study suggests that they cannot be straightforwardly interpreted in terms of static spontaneous fields arising from the unusual charge ordered state.

#### ACKNOWLEDGMENTS

This work was supported by the National Key R&D Program of China (2017YFA0303100), the Key R&D Program of Zhejiang Province, China (2021C01002), the National Natural Science Foundation of China (11874320, 12034017, 11974306, and 11974061), and the Zhejiang Provincial Natural Science Foundation of China (R22A0410240). S.K.G. acknowledges the Leverhulme Trust for support through the Leverhulme early career fellowship and thanks J. Quintanilla for discussions. Experiments at the ISIS Pulsed Neutron and Muon Source were supported by a beamtime allocation from the Science and Technology Facilities Council (RB2000246 [57] and RB2000245 [58]).

- 
- [1] L. Balents, Spin liquids in frustrated magnets, *Nature (London)* **464**, 199 (2010).
- [2] M. Fu, T. Imai, T.-H. Han, and Y. S. Lee, Evidence for a gapped spin-liquid ground state in a kagome Heisenberg antiferromagnet, *Science* **350**, 655 (2015).
- [3] T.-H. Han, J. S. Helton, S. Chu, D. G. Nocera, J. A. Rodriguez-Rivera, C. Broholm, and Y. S. Lee, Fractionalized excitations in the spin-liquid state of a kagome-lattice antiferromagnet, *Nature (London)* **492**, 406 (2012).
- [4] Z. Lin, J.-H. Choi, Q. Zhang, W. Qin, S. Yi, P. Wang, L. Li, Y. Wang, H. Zhang, Z. Sun, L. Wei, S. Zhang, T. Guo, Q. Lu, J.-H. Cho, C. Zeng, and Z. Zhang, Flatbands and Emergent Ferromagnetic Ordering in  $\text{Fe}_3\text{Sn}_2$  Kagome Lattices, *Phys. Rev. Lett.* **121**, 096401 (2018).
- [5] J.-X. Yin, S. S. Zhang, G. Chang, Q. Wang, S. S. Tsirkin, Z. Guguchia, B. Lian, H. Zhou, K. Jiang, I. Belopolski, N. Shumiya, D. Multer, M. Litskevich, T. A. Cochran, H. Lin, Z. Wang, T. Neupert, S. Jia, H. Lei, and M. Z. Hasan, Negative flat band magnetism in a spin-orbit-coupled correlated kagome magnet, *Nat. Phys.* **15**, 443 (2019).
- [6] M. Kang, L. Ye, S. Fang, J.-S. You, A. Levitan, M. Han, J. I. Facio, C. Jozwiak, A. Bostwick, E. Rotenberg, M. K. Chan, R. D. McDonald, D. Graf, K. Kaznatcheev, E. Vescovo, D. C. Bell, E. Kaxiras, J. van den Brink, M. Richter, M. P. Ghimire, J. G. Checkelsky, and R. Comin, Dirac fermions and flat bands in the ideal kagome metal  $\text{FeSn}$ , *Nat. Mater.* **19**, 163 (2020).
- [7] H.-M. Guo and M. Franz, Topological insulator on the kagome lattice, *Phys. Rev. B* **80**, 113102 (2009).
- [8] B. R. Ortiz, L. C. Gomes, J. R. Morey, M. Winiarski, M. Bordelon, J. S. Mangum, I. W. H. Oswald, J. A. Rodriguez-Rivera, J. R. Neilson, S. D. Wilson, E. Ertekin, T. M. McQueen, and E. S. Toberer, New kagome prototype materials: Discovery of  $\text{KV}_3\text{Sb}_5$ ,  $\text{RbV}_3\text{Sb}_5$ , and  $\text{CsV}_3\text{Sb}_5$ , *Phys. Rev. Materials* **3**, 094407 (2019).
- [9] B. R. Ortiz, S. M. L. Teicher, Y. Hu, J. L. Zuo, P. M. Sarte, E. C. Schueller, A. M. Milinda Abeykoon, M. J. Krogstad, S. Rosenkranz, R. Osborn, R. Seshadri, L. Balents, J. He, and S. D. Wilson,  $\text{CsV}_3\text{Sb}_5$ : A  $\mathbb{Z}_2$  Topological Kagome Metal with a Superconducting Ground State, *Phys. Rev. Lett.* **125**, 247002 (2020).
- [10] B. R. Ortiz, P. M. Sarte, E. M. Kenney, M. J. Graf, S. M. L. Teicher, R. Seshadri, and S. D. Wilson, Superconductivity in the  $\mathbb{Z}_2$  kagome metal  $\text{KV}_3\text{Sb}_5$ , *Phys. Rev. Materials* **5**, 034801 (2021).
- [11] Q. Yin, Z. Tu, C. Gong, Y. Fu, S. Yan, and H. Lei, Superconductivity and normal-state properties of kagome metal  $\text{RbV}_3\text{Sb}_5$  single crystals, *Chin. Phys. Lett.* **38**, 037403 (2021).
- [12] S.-Y. Yang, Y. Wang, B. R. Ortiz, D. Liu, J. Gayles, E. Derunova, R. Gonzalez-Hernandez, L. Šmejkal, Y. Chen, S. S. P. Parkin, S. D. Wilson, E. S. Toberer, T. McQueen, and M. N. Ali, Giant, unconventional anomalous Hall effect in the metallic frustrated magnet candidate,  $\text{KV}_3\text{Sb}_5$ , *Sci. Adv.* **6**, eabb6003 (2020).
- [13] F. H. Yu, T. Wu, Z. Y. Wang, B. Lei, W. Z. Zhuo, J. J. Ying, and X. H. Chen, Concurrence of anomalous Hall effect and charge

- density wave in a superconducting topological kagome metal, *Phys. Rev. B* **104**, L041103 (2021).
- [14] Y.-X. Jiang, J.-X. Yin, M. M. Denner, N. Shumiya, B. R. Ortiz, G. Xu, Z. Guguchia, J. He, M. S. Hossain, X. Liu, J. Ruff, L. Kautzsch, S. S. Zhang, G. Chang, I. Belopolski, Q. Zhang, T. A. Cochran, D. Multer, M. Litskevich, Z.-J. Cheng *et al.*, Unconventional chiral charge order in kagome superconductor  $\text{KV}_3\text{Sb}_5$ , *Nat. Mater.* **20**, 1353 (2021).
- [15] K. Y. Chen, N. N. Wang, Q. W. Yin, Y. H. Gu, K. Jiang, Z. J. Tu, C. S. Gong, Y. Uwatoko, J. P. Sun, H. C. Lei, J. P. Hu, and J.-G. Cheng, Double Superconducting Dome and Triple Enhancement of  $T_c$  in the Kagome Superconductor  $\text{CsV}_3\text{Sb}_5$  under High Pressure, *Phys. Rev. Lett.* **126**, 247001 (2021).
- [16] F. Du, S. S. Luo, B. R. Ortiz, Y. Chen, W. Duan, D. Zhang, X. Lu, S. D. Wilson, Y. Song, and H. Q. Yuan, Pressure-induced double superconducting domes and charge instability in the kagome metal  $\text{KV}_3\text{Sb}_5$ , *Phys. Rev. B* **103**, L220504 (2021).
- [17] Z. Zhang, Z. Chen, Y. Zhou, Y. Yuan, S. Wang, J. Wang, H. Yang, C. An, L. Zhang, X. Zhu, Y. Zhou, X. Chen, J. Zhou, and Z. Yang, Pressure-induced reemergence of superconductivity in the topological kagome metal  $\text{CsV}_3\text{Sb}_5$ , *Phys. Rev. B* **103**, 224513 (2021).
- [18] X. Chen, X. Zhan, X. Wang, J. Deng, X.-B. Liu, X. Chen, J.-G. Guo, and X. Chen, Highly robust reentrant superconductivity in  $\text{CsV}_3\text{Sb}_5$  under pressure, *Chin. Phys. Lett.* **38**, 057402 (2021).
- [19] Q. Wang, P. Kong, W. Shi, C. Pei, C. Wen, L. Gao, Y. Zhao, Q. Yin, Y. Wu, G. Li, H. Lei, J. Li, Y. Chen, S. Yan, and Y. Qi, Charge density wave orders and enhanced superconductivity under pressure in the kagome metal  $\text{CsV}_3\text{Sb}_5$ , *Adv. Mater.* **33**, 2102813 (2021).
- [20] N. N. Wang, K. Y. Chen, Q. W. Yin, Y. N. N. Ma, B. Y. Pan, X. Yang, X. Y. Ji, S. L. Wu, P. F. Shan, S. X. Xu, Z. J. Tu, C. S. Gong, G. T. Liu, G. Li, Y. Uwatoko, X. L. Dong, H. C. Lei, J. P. Sun, and J.-G. Cheng, Competition between charge-density-wave and superconductivity in the kagome metal  $\text{RbV}_3\text{Sb}_5$ , *Phys. Rev. Research* **3**, 043018 (2021).
- [21] F. H. Yu, D. H. Ma, W. Z. Zhuo, S. Q. Liu, X. K. Wen, B. Lei, J. J. Ying, and X. H. Chen, Unusual competition of superconductivity and charge-density-wave state in a compressed topological kagome metal, *Nat. Commun.* **12**, 3645 (2021).
- [22] F. Du, S. S. Luo, R. Li, B. R. Ortiz, Y. Chen, S. D. Wilson, Y. Song, and H. Q. Yuan, Evolution of superconductivity and charge order in pressurized  $\text{RbV}_3\text{Sb}_5$ , *Chin. Phys. B* **31**, 017404 (2022).
- [23] C. C. Zhao, L. S. Wang, W. Xia, Q. W. Yin, J. M. Ni, Y. Y. Huang, C. P. Tu, Z. C. Tao, Z. J. Tu, C. S. Gong, H. C. Lei, Y. F. Guo, X. F. Yang, and S. Y. Li, Nodal superconductivity and superconducting domes in the topological kagome metal  $\text{CsV}_3\text{Sb}_5$ , [arXiv:2102.08356](https://arxiv.org/abs/2102.08356) [cond-mat.supr-con].
- [24] W. Y. Duan, Z. Y. Nie, S. S. Luo, F. H. Yu, B. R. Ortiz, L. H. Yin, H. Su, F. Du, A. Wang, Y. Chen, X. Lu, J. J. Ying, S. D. Wilson, X. H. Chen, Y. Song, and H. Q. Yuan, Nodeless superconductivity in the kagome metal  $\text{CsV}_3\text{Sb}_5$ , *Sci. China Phys. Mech. Astron.* **64**, 107462 (2021).
- [25] R. Gupta, D. Das, C. H. Mielke III, Z. Guguchia, T. Shiroka, C. Baines, M. Bartkowiak, H. Luetkens, R. Khasanov, Q. Yin, Z. Tu, C. Gong, and H. Lei, Microscopic evidence for anisotropic multigap superconductivity in the  $\text{CsV}_3\text{Sb}_5$  kagome superconductor, *npj Quantum Mater.* **7**, 49 (2022).
- [26] L. C. Yin, D. T. Zhang, C. F. Chen, G. Ye, F. H. Yu, B. R. Ortiz, S. S. Luo, W. Y. Duan, H. Su, J. J. Ying, S. D. Wilson, X. H. Chen, H. Q. Yuan, Y. Song, and X. Lu, Strain-sensitive superconductivity in the kagome metals  $\text{KV}_3\text{Sb}_5$  and  $\text{CsV}_3\text{Sb}_5$  probed by point-contact spectroscopy, *Phys. Rev. B* **104**, 174507 (2021).
- [27] Z. Liang, X. Hou, F. Zhang, W. Ma, P. Wu, Z. Zhang, F. Yu, J.-J. Ying, K. Jiang, L. Shan, Z. Wang, and X.-H. Chen, Three-Dimensional Charge Density Wave and Surface-Dependent Vortex-Core States in a Kagome Superconductor  $\text{CsV}_3\text{Sb}_5$ , *Phys. Rev. X* **11**, 031026 (2021).
- [28] H.-S. Xu, Y.-J. Yan, R. Yin, W. Xia, S. Fang, Z. Chen, Y. Li, W. Yang, Y. Guo, and D.-L. Feng, Multiband Superconductivity with Sign-Preserving Order Parameter in Kagome Superconductor  $\text{CsV}_3\text{Sb}_5$ , *Phys. Rev. Lett.* **127**, 187004 (2021).
- [29] C. Mu, Q. Yin, Z. Tu, C. Gong, H. Lei, Z. Li, and J. Luo, s-wave superconductivity in kagome metal  $\text{CsV}_3\text{Sb}_5$  revealed by  $^{121/123}\text{Sb}$  NQR and  $^{51}\text{V}$  NMR measurements, *Chin. Phys. Lett.* **38**, 077402 (2021).
- [30] D. Song, L. Zheng, F. Yu, J. Li, L. Nie, M. Shan, D. Zhao, S. Li, B. Kang, Z. Wu, Y. Zhou, K. Sun, K. Liu, X. Luo, Z. Wang, J. Ying, X. Wan, T. Wu, and X. Chen, Orbital ordering and fluctuations in a kagome superconductor  $\text{CsV}_3\text{Sb}_5$ , *Sci. China Phys. Mech. Astron.* **65**, 247462 (2022).
- [31] M. M. Denner, R. Thomale, and T. Neupert, Analysis of Charge Order in the Kagome Metal  $\text{AV}_3\text{Sb}_5$  ( $A = \text{K}, \text{Rb}, \text{Cs}$ ), *Phys. Rev. Lett.* **127**, 217601 (2021).
- [32] X. Feng, K. Jiang, Z. Wang, and J. Hu, Chiral flux phase in the kagome superconductor  $\text{AV}_3\text{Sb}_5$ , *Sci. Bull.* **66**, 1384 (2021).
- [33] H. Tan, Y. Liu, Z. Wang, and B. Yan, Charge Density Waves and Electronic Properties of Superconducting Kagome Metals, *Phys. Rev. Lett.* **127**, 046401 (2021).
- [34] T. Park, M. Ye, and L. Balents, Electronic instabilities of kagome metals: Saddle points and Landau theory, *Phys. Rev. B* **104**, 035142 (2021).
- [35] C. Mielke III, D. Das, J. X. Yin, H. Liu, R. Gupta, C. N. Wang, Y. X. Jiang, M. Medarde, X. Wu, H. C. Lei, J. J. Chang, P. Dai, Q. Si, H. Miao, R. Thomale, T. Neupert, Y. Shi, R. Khasanov, M. Z. Hasan, H. Luetkens *et al.*, Time-reversal symmetry-breaking charge order in a kagome superconductor, *Nature (London)* **602**, 245 (2022).
- [36] L. Yu, C. Wang, Y. Zhang, M. Sander, S. Ni, Z. Lu, S. Ma, Z. Wang, Z. Zhao, H. Chen, K. Jiang, Y. Zhang, H. Yang, F. Zhou, X. Dong, S. L. Johnson, M. J. Graf, J. Hu, H.-J. Gao, and Z. Zhao, Evidence of a hidden flux phase in the topological kagome metal  $\text{CsV}_3\text{Sb}_5$ , [arXiv:2107.10714](https://arxiv.org/abs/2107.10714) [cond-mat.supr-con].
- [37] H. Li, S. Wan, H. Li, Q. Li, Q. Gu, H. Yang, Y. Li, Z. Wang, Y. Yao, and H.-H. Wen, No observation of chiral flux current in the topological kagome metal  $\text{CsV}_3\text{Sb}_5$ , *Phys. Rev. B* **105**, 045102 (2022).
- [38] A. Suter and B. Wojek, Musrfit: A free platform-independent framework for  $\mu\text{SR}$  data analysis, *Phys. Procedia* **30**, 69 (2012).
- [39] See Supplemental Material at <http://link.aps.org/supplemental/10.1103/PhysRevResearch.4.033145> for a comparison between fits of the 10-K ZF data with two fitting functions.
- [40] Z. Guguchia, C. Mielke III, D. Das, R. Gupta, J.-X. Yin, H. Liu, Q. Yin, M. Christensen, Z. Tu, C. Gong, N. Shumiya, Ts. Gamsakhurdashvili, M. Elender, P. Dai, A. Amato, Y. Shi, H. C.

- Lei, R. M. Fernandes, M. Z. Hasan, H. Luetkens *et al.*, Tunable nodal kagome superconductivity in charge ordered  $\text{RbV}_3\text{Sb}_5$ , [arXiv:2202.07713](https://arxiv.org/abs/2202.07713) [cond-mat.supr-con].
- [41] A. Géron, *Hands-on Machine Learning with Scikit-Learn, Keras, and TensorFlow: Concepts, Tools, and Techniques to Build Intelligent Systems* (O'Reilly Media, Sebastopol, CA, 2019).
- [42] T. Tula, G. Möller, J. Quintanilla, S. R. Giblin, A. D. Hillier, E. E. McCabe, S. Ramos, D. S. Barker, and S. Gibson, Machine learning approach to muon spectroscopy analysis, *J. Phys.: Condens. Matter* **33**, 194002 (2021).
- [43] T. Tula, G. Möller, J. Quintanilla, S. R. Giblin, A. D. Hillier, E. E. McCabe, S. Ramos, D. S. Barker, and S. Gibson, Joint machine learning analysis of muon spectroscopy data from different materials, in *Strongly Correlated Electron Systems (SCES) 2020 27/09/2021-01/10/2021 Campinas, Brazil, Journal of Physics Conference Series Vol. 2164* (Institute of Physics, London, 2022), p. 012018.
- [44] G. M. Luke, Y. Fudamoto, K. M. Kojima, M. I. Larkin, J. Merrin, B. Nachumi, Y. J. Uemura, Y. Maeno, Z. Q. Mao, Y. Mori, H. Nakamura, and M. Sgrist, Time-reversal symmetry-breaking superconductivity in  $\text{Sr}_2\text{RuO}_4$ , *Nature (London)* **394**, 558 (1998).
- [45] A. D. Hillier, J. Quintanilla, and R. Cywinski, Evidence for Time-Reversal Symmetry Breaking in the Noncentrosymmetric Superconductor  $\text{LaNiC}_2$ , *Phys. Rev. Lett.* **102**, 117007 (2009).
- [46] V. Grinenko, R. Sarkar, K. Kihou, C. H. Lee, I. Morozov, S. Aswartham, B. Büchner, P. Chekhonin, W. Skrotzki, K. Nenkov, R. Hühne, K. Nielsch, S. L. Drechsler, V. L. Vadimov, M. A. Silaev, P. A. Volkov, I. Eremin, H. Luetkens, and H.-H. Klauss, Superconductivity with broken time-reversal symmetry inside a superconducting *s*-wave state, *Nat. Phys.* **16**, 789 (2020).
- [47] P. K. Biswas, H. Luetkens, T. Neupert, T. Stürzer, C. Baines, G. Pascua, A. P. Schnyder, M. H. Fischer, J. Goryo, M. R. Lees, H. Maeter, F. Brückner, H.-H. Klauss, M. Nicklas, P. J. Baker, A. D. Hillier, M. Sgrist, A. Amato, and D. Johrendt, Evidence for superconductivity with broken time-reversal symmetry in locally noncentrosymmetric  $\text{SrPtAs}$ , *Phys. Rev. B* **87**, 180503(R) (2013).
- [48] T. Shang, M. Smidman, A. Wang, L.-J. Chang, C. Baines, M. K. Lee, Z. Y. Nie, G. M. Pang, W. Xie, W. B. Jiang, M. Shi, M. Medarde, T. Shiroka, and H. Q. Yuan, Simultaneous Nodal Superconductivity and Time-Reversal Symmetry Breaking in the Noncentrosymmetric Superconductor  $\text{CaPtAs}$ , *Phys. Rev. Lett.* **124**, 207001 (2020).
- [49] E. M. Kenney, B. R. Ortiz, C. Wang, S. D. Wilson, and M. J. Graf, Absence of local moments in the kagome metal  $\text{KV}_3\text{Sb}_5$  as determined by muon spin spectroscopy, *J. Phys.: Condens. Matter* **33**, 235801 (2021).
- [50] Y. Aoki, A. Tsuchiya, T. Kanayama, S. R. Saha, H. Sugawara, H. Sato, W. Higemoto, A. Koda, K. Ohishi, K. Nishiyama, and R. Kadono, Time-Reversal Symmetry-Breaking Superconductivity in Heavy-Fermion  $\text{PrOs}_4\text{Sb}_{12}$  Detected by Muon-Spin Relaxation, *Phys. Rev. Lett.* **91**, 067003 (2003).
- [51] N. Ratcliff, L. Hallett, B. R. Ortiz, S. D. Wilson, and J. W. Harter, Coherent phonon spectroscopy and interlayer modulation of charge density wave order in the kagome metal  $\text{CsV}_3\text{Sb}_5$ , *Phys. Rev. Materials* **5**, L111801 (2021).
- [52] Z. X. Wang, Q. Wu, Q. W. Yin, C. S. Gong, Z. J. Tu, T. Lin, Q. M. Liu, L. Y. Shi, S. J. Zhang, D. Wu, H. C. Lei, T. Dong, and N. L. Wang, Unconventional charge density wave and photoinduced lattice symmetry change in the kagome metal  $\text{CsV}_3\text{Sb}_5$  probed by time-resolved spectroscopy, *Phys. Rev. B* **104**, 165110 (2021).
- [53] S. Mañas-Valero, B. M. Huddart, T. Lancaster, E. Coronado, and F. L. Pratt, Quantum phases and spin liquid properties of  $1\text{T-TaS}_2$ , *npj Quantum Mater.* **6**, 69 (2021).
- [54] Y.-P. Lin and R. M. Nandkishore, Multidome superconductivity in charge density wave kagome metals, [arXiv:2107.09050](https://arxiv.org/abs/2107.09050) [Phys. Rev. B (to be published 2022)].
- [55] S. K. Ghosh, M. Smidman, T. Shang, J. F. Annett, A. D. Hillier, J. Quintanilla, and H. Q. Yuan, Recent progress on superconductors with time-reversal symmetry breaking, *J. Phys.: Condens. Matter* **33**, 033001 (2021).
- [56] X. Wu, T. Schwemmer, T. Müller, A. Consiglio, G. Sangiovanni, D. Di Sante, Y. Iqbal, W. Hanke, A. P. Schnyder, M. M. Denner, M. H. Fischer, T. Neupert, and R. Thomale, Nature of Unconventional Pairing in the Kagome Superconductors  $\text{AV}_3\text{Sb}_5$  ( $A = \text{K}, \text{Rb}, \text{Cs}$ ), *Phys. Rev. Lett.* **127**, 177001 (2021).
- [57] M. Smidman, D. T. Adroja, Y. Song, and S. P. Cottrell, Detecting a possible chiral flux phase in the kagome metal  $\text{CsV}_3\text{Sb}_5$ , STFC ISIS Neutron and Muon Source, 2021, <https://doi.org/10.5286/ISIS.E.RB2000246>.
- [58] S. K. Ghosh, A. D. Hillier, and P. K. Biswas, New paradigm of unconventional superconductivity in the newly discovered topological kagome metal  $\text{CsV}_3\text{Sb}_5$ , STFC ISIS Neutron and Muon Source, 2021, <https://doi.org/10.5286/ISIS.E.RB2000245>.